2011-10-18

Structure, Thermodynamics, and Energy Content of Aluminum --Cyclopentadienyl Clusters

Hooper, Joseph P.

American Chemical Society

THE JOURNAL OF PHYSICAL CHEMISTRY A

ARTICLE

pubs.acs.org/JPCA

Structure, Thermodynamics, and Energy Content of Aluminum−Cyclopentadienyl Clusters

Kristen S. Williams[†,§] and Joseph P. Hooper*[,†,‡]

[†]Research Department, Naval Surface Warfare Center, Indian Head, Maryland 20640, United States

[‡]Department of Physics, Naval Postgraduate School, Monterey, California 93943, United States

[§]Materials Science and Engineering Program, Texas A&M University, College Station, Texas 77843, United States

ABSTRACT: We present quantum chemistry simulations of aluminum clusters surrounded by a surface layer of cyclopentadiene-type ligands to evaluate the potential of such complexes as novel fuels or energetic materials. Density functional theory simulations are used to examine the aluminum-ligand bonding and its variation as the size of the aluminum cluster increases. The organometallic bond at the surface layer arises mainly from ligand charge donation into the Al *p* orbitals balanced with repulsive polarization effects. Functionalization of the ligand and changes in Al cluster size are found to alter the relative balance of these effects, but the surface organometallic bond generally remains stronger than Al−Al bonds elsewhere in the cluster. In large clusters, such as the experimentally observed $Al_{50}Cp_{12}^*$, this suggests that unimolecular thermal decomposition likely proceeds through loss of surface AlCp* units, exposing the strained interior aluminum core. The calculated heats of combustion per unit volume for these systems are high, approaching 60% that of pure aluminum. We discuss the possibility of using organometallic aluminum clusters as a means of achieving rapid combustion in propellants and fuels.

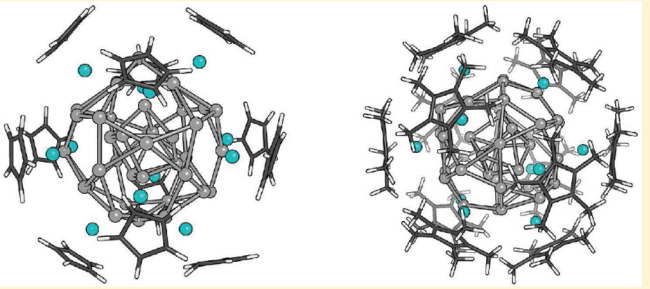

INTRODUCTION

Modern solid rocket propellants frequently use aluminum powder as a fuel component due to its high enthalpy of combustion. These powders are generally of micrometer size, but in recent years there has been significant study of nanometer scale Al as a route to increasing the oxidation rates and potentially lowering the ignition threshold.[1,2] The outer surface of the aluminum grains consists of an oxidized alumina layer ∼2−6 nm thick, which can limit rapid reactivity of the internal Al.[3] This has led several authors to pursue surface passivation of aluminum nanoparticles with organic functional groups that prevent formation of the oxide.[3−6] However, larger nanoparticles of aluminum will still have oxidation rates limited by the diffusion of fuel to the detached flame front and the agglomeration of condensed aluminum oxide during combustion.[7]

To this end, we have been pursuing the possibility of molecular-scale aluminum clusters with a protective organic layer as novel additives for solid rocket motor propellant formulations. As an example of such a material, H. Schnöckel and co-workers have previously synthesized a 50-atom Al cluster surrounded by cyclopentadienyl Cp* ($C_5[CH_3]_5$) ligands.[8] The metal−ligand (M-L) interaction on the exterior of the cluster consists of η^5 bonds between the Al and the Cp* rings. Their study of larger aluminum clusters builds on a large body of work on low-valence aluminum coordination complexes.[9−13] A number of these clusters, such as the tetramers $Al_4Cp_4^*$ and $Al_4(C_5Me_4H)_4$, crystallize into low-symmetry solid state structures and have been observed via X-ray crystallographic analysis and NMR spectroscopy.[14,15] Attempts to isolate similar compounds with unmethylated Cp (C_5H_5) ligands have generally been unsuccessful due to their tendency to disproportionate to aluminum metal and higher-valence compounds such as $AlCp_3$.[11,14] Currently very little is known about the stability or decomposition of the larger aluminum−cyclopentadienyl compounds that contain a significant mass fraction of aluminum.

Computational studies on these materials are limited and mainly restricted to work on aluminum metallocenes. Early Hartree−Fock calculations by Ahlrichs and co-workers[16] examined basic AlCp as well as Al_4Cl_4, Al_4F_4, and Al_4Cp_4. No correlation effects were included, and with their methodology, Al_4Cp_4 was found to be unstable with respect to decomposition into monomers. A number of later works considered the simple Al metallocenes in the context of examining trends in a broader range of main-group metallocenes or similar organometallics.[17−20] In recent years, Huber and Schnöckel have performed density functional theory calculations in support of their X-ray diffraction and ^{27}Al NMR studies of larger aluminum−Cp-type clusters.[14,21] They proposed that the large clusters, such as $Al_{50}Cp_{12}^*$, may serve as a type of barrier state that prevents the smaller compounds from spontaneously decomposing to metallic aluminum and trivalent aluminum species. Expanded computational studies of these materials are highly

Received: July 30, 2011
Revised: October 4, 2011
Published: October 18, 2011

Table 1. Calculated Bond Lengths and Distances of Half-Metallocene Complexes[a]

cluster	C−C bond length (Å)	Al−X distance (Å)	slip (Å)	hapticity
AlCp	1.420	2.064	0.002	η^5
ref 16	1.409	2.039		
ref 17	1.420	2.037		
ref 18	1.428	2.059		
ref 19		2.06		
ref 20		2.05		
AlCp*	1.429	2.021	0.000	η^5
ref 17	1.498	1.989		
ref 27[b]	1.414	2.063		
$AlC_5H_4NO_2$	1.417	2.116	0.003	η^5
$AlC_5Me_4CF_3$	1.428	2.053	0.058	η^5
$AlC_5[CF_3]_5$	1.425	2.216	0.031	η^5

[a] Average slip and ligand hapticity are calculated by perpendicular projection of Al atoms onto the Cp-type rings. Al−X distances are only calculated for species with η^5 bonding. [b] Experimental data.

Table 2. Calculated Average Bond Lengths and Distances of Larger Al−Cp Clusters

cluster	C−C bond length (Å)	Al−X distance (Å)	slip (Å)	hapticity
$AlCp_3$	1.424		1.083	η^2
			1.546	η^1
			1.738	η^1
$AlCp_3$*	1.439		0.958	η^2
			2.168	η^1
			2.318	η^1
Al_4Cp_4	1.420	2.072	0.003	η^5
ref 16	1.408	2.056		
ref 17	1.408			
ref 20		2.06		
ref 14	1.429	2.052		
Al_4Cp_4*	1.428	2.073	0.033	η^5
ref 14[a]	1.437	2.059		
ref 9[a]		2.015		
Al_8Cp_4	1.421	2.000	0.006	η^5
Al_8Cp_4*	1.432	1.956	0.005	η^5
$Al_{50}Cp_{12}$	1.442		1.231	η^1
	1.437	1.992	0.00	η^5
$Al_{50}Cp_{12}$*	1.429	2.064	0.209	η^5
QM/MM[b]	1.429	2.121		
ref 8[a]	1.421	1.981		

[a] Experimental data. [b] QM/MM refers to geometry optimization of the largest cluster ($Al_{50}Cp_{12}$*) with the multilayer method B3LYP/6-31 g(d,p):UFF.

desirable to elucidate their reactivity, stability, and potential combustion properties.

In this work we present first-principles calculations of the structure, thermodynamics, and energy content of these aluminum cluster materials, with a particular focus on their possible role as rapidly combusting fuels or propellants. We examine their structure and chemical bonding, steric hindrance, thermodynamics, and likely initial decomposition steps. Using calculated thermodynamic data, we examine the proposed mechanism for the stability of these clusters discussed above and show that our calculations are in disagreement with this mechanism. We also estimate the energy release potential of these clusters, comparing heats of combustion and specific impulses to other common propellant ingredients to examine their possible utility as rapidly burning fuels.

COMPUTATIONAL METHODOLOGY

Calculations on aluminum organometallic clusters are performed using density functional theory with the B3LYP functional[22] and a 6-31G(d,p) basis set. For comparison and assurance of accurate thermodynamic values, we also calculate heats of formation using the G2 method[23] for a number of the smaller clusters. B3LYP/6-31G(d,p) gives accurate thermodynamics while still being efficient enough to calculate structures and vibrational properties of the large clusters (350 atoms). All calculations are performed with the Gaussian 09 program[24] at the AFRL supercomputing center. For geometry optimization of the largest cluster, $Al_{50}Cp_{12}$*, a multilayer QM/MM method[25] is used in which the methyl groups on each Cp* ligand are modeled with Rappe's Universal Force Field (UFF)[26] and remaining atoms are treated with DFT. Layer neutrality is automatically imposed such that the dangling bonds in each layer are passivated with hydrogen. This hybrid approach is only used in finding optimized geometries of $Al_{50}Cp_{12}$*; thermodynamic calculations are then performed with a full DFT calculation at the B3LYP/UFF geometry. The small structural differences between the QM/MM and full DFT approach have a minimal effect on calculated energy difference or enthalpies of formation. As discussed below, the energy barrier for rotation of the outer methyl groups is extremely small and the contribution of the methyl vibrations to the thermodynamic partition function is negligible.

RESULTS AND DISCUSSION

Structure and Bonding. We first present results on the theoretical structure of aluminum complexes bound to cyclopentadienyl type ligands. In Table 1 we list the calculated B3LYP/6-31G(d,p) bond lengths for half-metallocene configurations of Al with Cp and related derivatives. In addition to providing insight into the individual Al-L bonding, these structures also form the protective outer layer on the larger aluminum clusters discussed below. The distance from the Al to the center of the Cp ring (Al-X) is given, along with the C−C bond length in the ring. The C−C bond lengths presented are averaged over all intraring carbons. The Al-ring center distances are obtained via perpendicular projection of Al onto the plane of the C_5 ring. The absolute difference between this projection and the ring center is defined as the ring slip. Our calculated slip values are then used to assign hapticities in accordance with the study of main-group half metallocenes by Budzelaar and co-workers:[19] η^5, 0 Å; η^3, 0.8 Å; η^2, 1.0 Å; η^1, ≥1.2 Å. Our calculated geometries for AlCp are in good agreement with other recent studies of main-group metallocenes, such as that by Rayon and Frenking.[18] In addition, we consider three substituted Cp derivatives; nitro-Cp ($C_5H_4NO_2$), trifluoromethyl-Cp* ($C_5Me_4CF_3$), and pentatrifluoromethyl-Cp* ($C_5[CF_3]_5$). The substituted Cp ligands allow us to examine the M-L bond strength with various electron withdrawing groups that may also serve as oxidizers for the

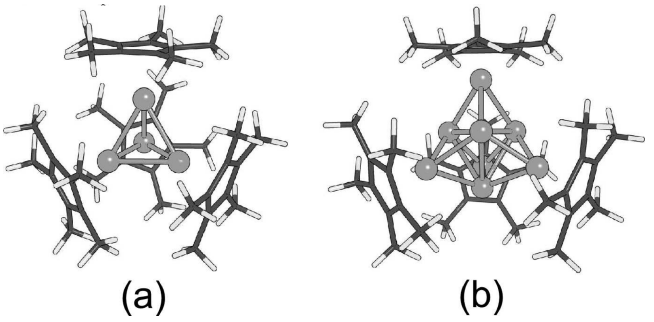

Figure 1. Calculated structures of (a) $Al_4Cp_4^*$ and (b) $Al_8Cp_4^*$.

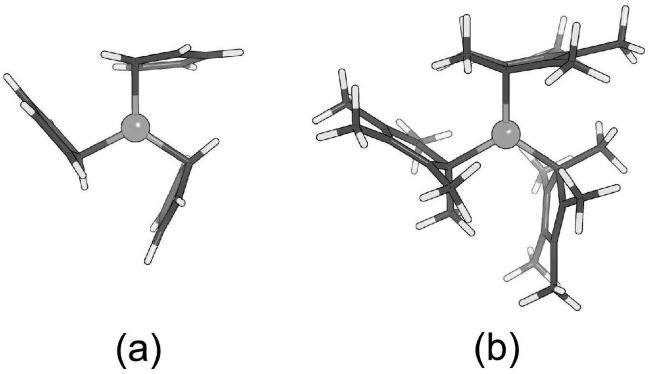

Figure 2. Comparison of groundstate geometries of (a) $AlCp_3$ and (b) $AlCp_3^*$. The symmetry of the Cp* ring is broken in (b), as the methyl groups bend out of the ring plane due to the significant steric hindrance.

aluminum complexes during thermal decomposition. All substituted Cp ligands result in only slight shifts of the Al (<0.06 Å) and essentially retain the η^5 configuration of standard AlCp. The Al-ring distance increases slightly with the addition of electron withdrawing groups to the Cp ring; further discussion of the M-L bond changes in these substituted complexes is given below.

We next consider larger clusters composed of an AlCp or AlCp* shell surrounding an aluminum core. As our ultimate interest is in materials with a significant mass fraction of combustible aluminum, our focus is on the larger, experimentally observed $Al_{50}Cp_{12}^*$ cluster and related compounds that help to clarify its properties. Table 2 contains averaged bond lengths and distances for each optimized structure along with previous experimental and theoretical values where available. Figures 1−3 show the calculated geometries of the complexes. Of the compounds listed, only $Al_4Cp_4^*$, $AlCp_3$, $AlCp_3^*$, and $Al_{50}Cp_{12}^*$ have characterized solid-state structures. $Al_8Cp_4^*$ is observed in laser desorption mass spectrometry of solid-state $Al_4Cp_4^*$ and represents an intermediate between the tetramer and the large Al_{50} complex.[28] The remaining compounds in Table 2 are part of a reaction scheme proposed by Schnöckel and co-workers to explain the formation and stability of the large aluminum clusters.[21] All of our calculated values agree with available previous results to within 0.1 Å. Furthermore, the QM/MM multilayer calculation on the largest cluster does quite well in reproducing the geometry obtained using full B3LYP; the C−C intraring distances are identical, and the Al−X distance is within 0.06 Å. The calculated Al-ring distances in $Al_{50}Cp_{12}^*$ are slightly larger than experiment due to the lack of a condensed phase environment in the calculation. The hapticity of the M−L

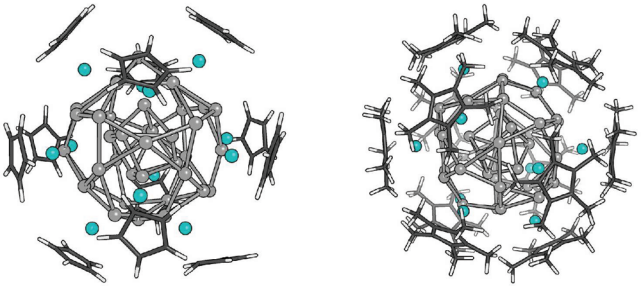

Figure 3. Calculated structures of $Al_{50}Cp_{12}$ (left) and $Al_{50}Cp_{12}^*$ (right). Surface aluminum atoms directly involved in organometallic bonding are shown in teal.

Table 3. Average Distances between Al Atoms Located in the Interior Cages of the Clusters[a]

cluster	cage	Al−Al distance (Å)
Al_4	Al_4	2.795
Al_4Cp_4	Al_4	2.764
$Al_4Cp_4^*$	Al_4	2.869 (*2.767*)[b]
Al_8Cp_4	Al_4 shell	2.788
	Al_4 caps	2.675
$Al_8Cp_4^*$	Al_4 shell	2.805
	Al_4 caps	2.673
$Al_{50}Cp_{12}$	Al_8 shell	2.69
	$Al_{30}-Al_{12}$	2.812 (η^1) 3.041 (η^5)
	diameter	15.314
$Al_{50}Cp_{12}^*$	Al_8 shell	2.690 (*2.664*)[b]
	$Al_{30}-Al_{12}$	2.947 (*2.867*)[b]
	diameter	15.241 (*14.896*)

[a] Experimental values given in italics. [b] Ref 8.

bonds in these compounds is generally η^5, with two exceptions. The first is the $AlCp_3$ and $AlCp_3^*$ systems, which contain trivalent aluminum and exhibit significant steric interaction between the ligands (see Figure 2). The second is the $Al_{50}Cp_{12}$ cluster with its unmethylated ligands, in which 8 of the 12 binding ligands shift to an η^1 position (Figure 3). In systems with mixed hapticities, all bonding configurations are listed in Table 2.

In Table 3 we list average cluster spacings, with the larger clusters broken up into cages to examine how the bond lengths change in the interior regions. The interior Al_8 core of the $Al_8Cp_4/Al_8Cp_4^*$ clusters is broken into two cages: an innermost tetrahedral Al_4 shell and the four exterior Al_4 units that cap its faces. Bond lengths in the innermost Al_4 shells are longer than in the Al_4 exterior tetrahedral caps, regardless of the choice of ligand. The effect of substituting Cp* for Cp is the same as in the smaller Al_4 cluster; Cp* slightly increases the average Al−Al bond length in the innermost shell.

The large $Al_{50}Cp_{12}^*$ cluster has been discussed in a number of papers by Schnöckel and co-workers.[8,13] Our calculated structure for this compound is given in Figure 3, along with the theoretical geometry of the unmethylated (and experimentally unobserved) analog $Al_{50}Cp_{12}$. Both compounds are divided into the following pieces: an inner Al_8 shell, an exterior Al_{12} shell that is shown in teal and consists of the Al atoms bound directly to ligands, and a final Al_{30} shell between these. As noted above, 8 of the 12 ligands in the $Al_{50}Cp_{12}$ system change

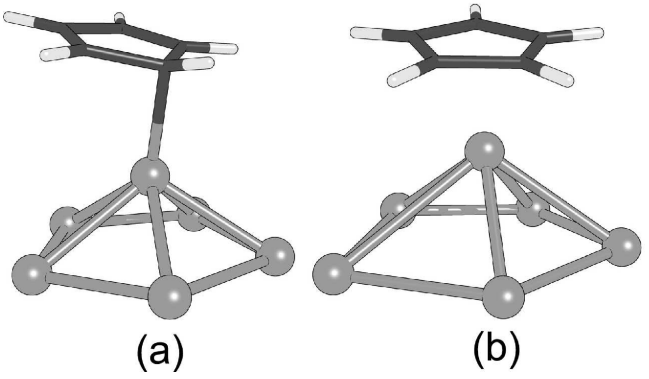

Figure 4. Two bonding motifs at the $Al_{50}Cp_{12}$ surface: (a) η^1 and (b) η^5.

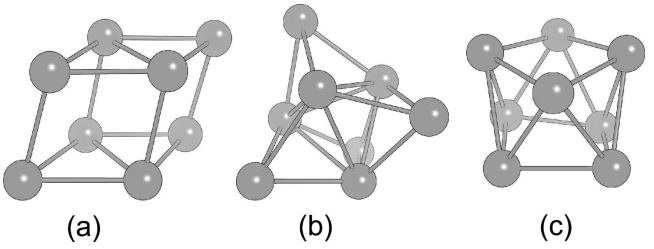

Figure 5. (a) Ground-state geometry of the neutral, bare Al_8 cluster; (b) the Al_8 core of $Al_8Cp_4^*$; (c) the distorted Al_8 core of $Al_{50}Cp_{12}^*$.

hapticity (shown in Figure 4). Bonds in the Al_8 interior shells are shorter than those connecting the Al_{30} and Al_{12} shells, which is opposite the behavior seen in the smaller Al_4 and Al_8 clusters. All of our calculated averages agree with experimental results for the $Al_{50}Cp_{12}^*$ solid state structure, including the effective cluster diameter. This is defined as twice the radius, with the radius being the average distance from the cluster center to the plane of the Cp* ring. The innermost Al_8 cluster of $Al_{50}Cp_{12}^*$ is shown in Figure 5, along with the Al_8 core of $Al_8Cp_4^*$ and an isolated Al_8 cluster. The latter is in agreement with previous calculations of small aluminum clusters by Rao and Jena.[29] Al atoms in both of the organometallic clusters (b and c) arrange differently than in the bare cluster; the interior Al core of $Al_{50}Cp_{12}$ is similar to that in the methylated version (c) as well, and both have significantly lowered symmetry compared to an isolated cluster (a). Very recent work by Schnöckel and co-workers provides some additional discussion on the asymmetry of the Al_8 core in relation to recently synthesized organometallic gold clusters.[30]

We next consider in more detail the nature of the metal−ligand bond in Al−Cp complexes. It is instructive to examine the simple AlCp half-metallocene, as all the Al−Cp bonds in larger systems considered here display similar features. While AlCp ostensibly follows an octet rule (5 e^- from Cp and 3 e^- from Al), electron counting heuristics are generally a poor guide to main-group metallocene compounds.[31] Instead, we consider directly the bonding molecular orbitals (MOs) and fragment interaction. Similar to previous treatments, we separate the system into Al^+ and Cp^- fragments. This is consistent with the energy decomposition analysis of Rayon and Frenking[18] and the study of Budzelaar and co-workers[19] examining the basic AlCp half-metallocene; both conclude that the character of the AlCp bond is predominantly ionic. It is also consistent with the NBO partial

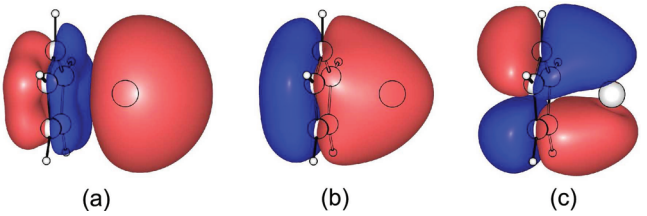

Figure 6. Three relevant bonding MOs for AlCp: (a) the HOMO, which consists of the nonbonding interaction between the Cp a_1 and the Al *sp*; (b) the HOMO-7, showing the Cp a_1 bonding interaction with Al *sp*; (c) The HOMO-1, showing overlap between the Al *p* and the Cp e_1.

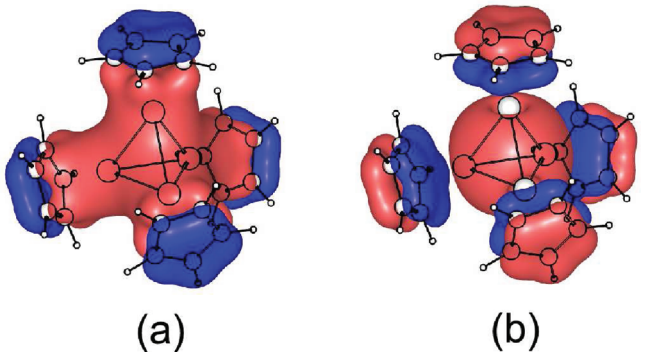

Figure 7. Bonding MOs for Al_4Cp_4, showing favorable overlap of the half-metallocene MOs leading to bonding in the interior Al tetramer.

charges observed on all our η^5 compounds (see below for more discussion).

Four orbitals, three of which are shown in Figure 6, comprise the majority of the bonding character in AlCp. The a_1 Cp orbital bonds with one *sp* from the aluminum, with the nonbonded lone-pair residing in the remaining *sp*, which is also the HOMO. The two filled e_1 orbitals on Cp form two degenerate bonding orbitals with two unfilled aluminum *p* orbitals. The surface Al-ligand units in larger clusters also bond via analogous MOs; an example is shown for the Al_4Cp_4 system in Figure 7, in which favorable overlap of the Al *sp* orbitals gives rise to a weak bonding in the inner aluminum tetrahedron.

To get a quantitative sense of the contribution from different orbitals, we perform a charge decomposition analysis (CDA)[32] to examine the charge donation from the ligand to the Al^+. CDA constructs the wave function of the M−L compound in terms of the linear combination of the donor and acceptor fragment orbitals. Each molecule is decomposed into closed-shell fragments corresponding to the Al^+ (denoted M) and the ligand anion (denoted L).

The bonding in each orbital can be characterized by three terms: L → M charge donation, M → L back-donation, and charge polarization (or mixing of the occupied orbitals of both M and L). The results of CDA analysis on five Al metallocenes with various functional groups on the Cp ligand are given in Table 4. The columns of Table 4 contain the relative amount of donation (*d*) and charge repulsion (*r*), or polarization, in each molecule. There are small negative values (on the order of −0.15) for the back-donation, which likely arise from small repulsion effects that are also included in the methodology for calculating this term.[32] In the ionic configuration studied, we expect no true back-bonding such as occurs in typical transition metal metallocenes;

Table 4. CDA Results for the Bonding Orbitals of Half-Sandwich Al Metallocenes with Various Cp Derivatives[a]

	AlCp		AlCp*		$AlC_5H_4NO_2$		$AlC_5Me_4CF_3$		$AlC_5[CF_3]_5$	
orbital	*d*	*r*	*d*	*r*	*d*	*r*	*d*	*r*	*d*	*r*
Al *sp* nonbonded	0.359	−1.655	0.388	−1.736	0.312	−1.571	0.357	−1.675	0.205	−1.424
Cp $e_1 \cdots$ Al p_x	0.530	−0.004	0.455	−0.004	0.481	−0.003	0.427	−0.004	0.316	−0.002
Cp $e_1 \cdots$ Al p_y	0.531	−0.004	0.455	−0.004	0.397	−0.012	0.432	−0.022	0.328	−0.002
Cp $a_1 \cdots$ Al *sp*	0.187	0.552	0.087	0.214	0.188	0.483	0.086	0.173	0.125	0.348
total (all orbitals)	1.892	−1.046	1.876	−1.146	1.643	−1.002	1.773	−1.119	1.347	−0.922

[a] The columns are forward electron donation (*d*) and charge repulsion (*r*).

Table 5. NBO Partial Charges on the Al Atoms Bound to Ligand Groups and HOMO−LUMO Gaps for All Clusters[a]

molecule	*q* (NBO)	*q*/*q*(AlCp)	gap (eV)
AlCp	0.630[b]	1.00	5.72
AlCp*	0.657	1.04	5.49
$AlC_5H_4NO_2$	0.700	1.11	4.46
$AlC_5Me_4CF_3$	0.689	1.09	5.57
$AlC_5[CF_3]_5$	0.774	1.23	6.14
$AlCp_3$	1.870	2.97	4.21
$AlCp_3$*	1.908	3.03	4.61
Al_4Cp_4	0.591	0.94	4.61
Al_4Cp_4*	0.641	1.02	4.36
Al_8Cp_4	0.693	1.10	2.99
Al_8Cp_4*	0.760	1.21	3.12
$Al_{50}Cp_{12}$	0.724 (η^1)	1.15 (η^1)	1.43
	0.901 (η^5)	1.43 (η^5)	
$Al_{50}Cp_{12}$*	0.913	1.45	1.57

[a] Charges for clusters with multiple Al atoms are averaged over all Al atoms participating in metal−ligand bonds (i.e., 4 atoms for Al_4Cp_4*, 4 for Al_8Cp_4*, and 12 for $Al_{50}Cp_{12}$*). [b] A previous NBO atomic partial charge of 0.61 is published in ref 18 and 33.

thus, this quantity is not listed in the table. Actual charge values from the CDA analysis are not important,[32] and we focus instead on the relative amounts of forward donation and repulsion.

The CDA analysis suggests that the bonding character can be viewed as a balance between forward donation into the aluminum *p* orbitals and repulsion from polarization effects. In the simple case of AlCp, the former arises primarily from donation from the Cp e_1 to Al *p* and the latter mainly from repulsion between the Al lone pair and the Cp a_1. All other functionalized AlCp complexes are also dominated by orbitals that are analogous to the four bonding orbitals of bare AlCp. Table 4 lists the contributions from each of these orbitals as well as the total values of donation and repulsion.

For all variants listed in Table 4, the primary repulsive contribution arises from the HOMO, which contains the nonbonding Al *sp*. In the CDA analysis, negative values of *r* generally correspond to charge moving away from the bonding region between the donor and acceptor fragments. Similarly, a positive sign indicates an accumulation of charge in the same region. Approximately 50−55% of the total charge donated from the ligand to the metal is from orbitals analogous to the Cp e_1. The Al *sp* with a bonding overlap with the Cp a_1 generally contains a small amount of forward donation and a positive repulsion term. For the compounds with methyl type groups off the ligand (AlCp* and the fluorinated variants), there is also a small contribution from the sp^3 orbitals on the methyl carbons.

Comparing AlCp* to AlCp, we note that the presence of the additional methyl groups lowers the forward donation from the e_1 orbitals, though there is an additional donation from the methyl carbons, as mentioned previously. There is a slight increase in repulsive polarization with the nonbonding Al *sp*, but overall, there is little difference between Cp and Cp* in terms of donor/acceptor interactions. The remaining Cp derivatives all contain electron withdrawing groups, which lower both the donation and the repulsion terms and also result in slightly increased Al-ring bond lengths as compared to Cp and Cp* (see Table 1). The reduction in forward donation is the more dominant effect based on the CDA analysis. The effects of the substituents on the bond strength (via the bond dissociation energies in Table 6, discussed below) can also be qualitatively understood in terms of forward donation and repulsion. In $AlC_5[CF_3]_5$, for example, the electron withdrawing groups reduce both the forward donation and the repulsive polarization. These effects largely balance, giving an aluminum-ligand bond strength very similar to that of the basic AlCp system.

For making comparisons among the different molecules and clusters, the natural bond orbital (NBO) partial charges are given in Table 5. Also included in this table are the NBO charges normalized to the value for AlCp. Partial charges are not generally good indicators of valence,[31] but we do see a general trend that the trivalent $AlCp_3$ complexes have a partial charge three times that of the isolated metallocene, and the Al atoms bound to Cp/Cp* in the Al_{50} clusters have an intermediate charge between these. The HOMO−LUMO gap is also listed in Table 5, and we observe a steady decrease in the gap energy with increasing cluster size. Al_4Cp_4* has a value typical of insulators at 4.36 eV. Increasing the cluster size to 8 Al atoms decreases the HOMO−LUMO gap to 3.12 eV, and the largest Al_{50} systems are approaching semiconducting values at 1.43 and 1.57 eV. Very recently, Lopez-Acevedo and co-workers[34] and Clayborne and co-workers[35] have reported on aluminum as well as gold and gallium clusters, in the context of superatom models. Their partial charges and HOMO−LUMO gaps are consistent with the results presented here.

To analyze the relative bonding strength and possible unimolecular decomposition pathways in the systems, we next consider the bond dissociation energies (BDEs), defined as the reaction energy D_e for homolytic cleavage of the listed bond. The BDE adjusted with a zero-point correction (D_0) and the Gibbs free energy change of the reaction ΔG^0 at 298 K and 1 atm are also listed. BDEs for the half metallocene complexes are given in Table 6 and those of larger clusters are given in Table 7. The

Table 6. Bond Dissociation Energies for Several Reactions Involving Half-Metallocene Complexes[a]

eq	BDE reaction	D_e (kcal/mol)	D_0 (kcal/mol)	ΔG^0 (kcal/mol)
I	$Al_4 \rightarrow 4Al^{\bullet}$	107.30	105.89	88.11
II	$AlCp \rightarrow Al^{\bullet} + Cp^{\bullet}$	85.87	82.47	73.83
III	$AlCp^* \rightarrow Al^{\bullet} + [Cp^*]^{\bullet}$	76.81	74.13	65.58
IV	$AlC_5H_4NO_2 \rightarrow Al^{\bullet} + [C_5H_4NO_2]^{\bullet}$	81.53	79.08	70.36
V	$AlC_5Me_4CF_3 \rightarrow Al^{\bullet} + [C_5Me_4CF_3]^{\bullet}$	74.53	72.25	62.54
VI	$AlC_5[CF_3]_5 \rightarrow Al^{\bullet} + [C_5[CF_3]_5]^{\bullet}$	84.60	82.65	72.98

[a] D_e is calculated using only the DFT electronic energies, while D_0 includes a zero-point correction. ΔG^0 is defined as the Gibbs free energy of the reaction at 298 K and 1 atm.

Table 7. Bond Dissociation Energies for Several Reactions Involving Aluminum−Cyclopentadienyl Complexes and Clusters

eq	BDE reaction	D_e (kcal/mol)	D_0 (kcal/mol)	ΔG^0 (kcal/mol)
VII	$AlCp_3 \rightarrow Cp_2Al^{\bullet} + Cp^{\bullet}$	61.02	57.50	43.58
VIII	$AlCp_3^* \rightarrow Cp_2^*Al^{\bullet} + [Cp^*]^{\bullet}$	28.59	24.96	10.07
IX	$Al_4Cp_4 \rightarrow Cp_3Al_4^{\bullet} + Cp^{\bullet}$	62.60	59.67	48.91
X	$Al_4Cp_4^* \rightarrow Cp_3^*Al_4^{\bullet} + [Cp^*]^{\bullet}$	44.89	41.30	24.75
XI	$Al_4Cp_4 \rightarrow 4AlCp$	16.09	15.04	−17.75
XII	$Al_4Cp_4^* \rightarrow 4AlCp^*$	9.09	7.39	−35.14
XIII	$Al_8Cp_4 \rightarrow Cp_3Al_8^{\bullet} + Cp\cdot$	54.88	51.58	39.08
XIV	$Al_8Cp_4 \rightarrow Cp_3Al_7 + AlCp$	32.37	31.03	17.36
XV	$Al_8Cp_4^* \rightarrow Cp_3^*Al_8^{\bullet} + [Cp^*]^{\bullet}$	47.52	44.47	28.49
XVI	$Al_8Cp_4^* \rightarrow Cp_3^*Al_7 + AlCp^*$	37.39	37.69	18.43
XVII	$Al_{50}Cp_{12} \rightarrow Cp_{11}Al_{50}\cdot + [Cp]^{\bullet}$	53.76		
XVIII	$Al_{50}Cp_{12} \rightarrow Cp_{11}Al_{49}^{\bullet} + AlCp$	28.61		
XIX	$Al_{50}Cp_{12}^* \rightarrow Cp_{11}^*Al_{50}^{\bullet} + [Cp^*]^{\bullet}$	79.72		
XX	$Al_{50}Cp_{12}^* \rightarrow Cp_{11}^*Al_{49}^{\bullet} + AlCp$	58.30		

substituted Cp derivatives all lower the BDE as compared to AlCp, though the largest effect (for the Cp* with a single methyl replaced by a fluoro group) only reduces the bond strength by 13%. Possible substitutions with oxidizing groups, thus, do not radically change the basic monovalent bond with aluminum, but naturally there may be significant differences in terms of solvent effects or unintended oxidation of the aluminum clusters.

We next discuss the Al_4 clusters shown in Table 7. The BDE associated with removing one Cp ligand from Al_4Cp_4 is 62.60 kcal/mol, while the tetramerization energy is 16.09 kcal/mol. This implies that the M−L bond is much stronger than the Al−Al bonds, as would be expected. The same is true for $Al_4Cp_4^*$, where the M−L BDE of 44.89 kcal/mol is much higher than the tetramerization energy of 9.09 kcal/mol. Previous calculations by Huber and Schnöckel using BP86 and an SVP basis set also showed that Al_4Cp_4 is more stable against decomposition into monomers than $Al_4Cp_4^*$.[14] The experimentally estimated value for the tetramerization energy in solution based on[27] Al NMR is approximately 36 kcal/mol;[9] we note that the gas phase energy barrier is expected to be lower than the condensed phase value due to solvent and steric effects; thus, it is difficult to directly compare tetrametrization energies with the NMR estimate.

We note that no stable structure was found computationally for Al_3Cp_3 following removal of a full AlCp unit. The favored decomposition pathway will be dissociation into four AlCp or AlCp* monomers. This is further supported by the ΔG^0 values given in column 4 of 7. ΔG^0 is negative for eqs and , indicating that the barrier to decomposition of the isolated cluster at ambient conditions is minimal. We, thus, expect that $Al_4Cp_4^*$ will depend very heavily on steric interactions with the solvent or adjacent clusters for its stability.

We next consider M−L bond strength in the larger Al_8 clusters. The trends are similar; namely, the BDE to remove one Cp ligand from Al_8Cp_4 is 54.88 kcal/mol, while the BDE for removal of an entire AlCp monomer is 32.37 kcal/mol. The relative difference between the two is not as large as in the Al_4Cp_4 cluster, but the trend is the same. Also, the M−L BDE of $Al_8Cp_4^*$ is 47.52 kcal/mol, which is again slightly larger than the monomer BDE of 37.39 kcal/mol. For the largest cluster, $Al_{50}Cp_{12}^*$, we consider only D_e for computational efficiency. The BDE for the M−M bond between Al atoms in the Al_{38} shell and the Al_{12} shell is only 58.30 kcal/mol compared with the M−L bond BDE of 79.72 kcal/mol.

Lastly, we comment on the general behavior of the M−L bond. First, the strength of the M−L BDE of surface AlCp units remains generally constant with cluster size. In fact, the BDE associated with breaking the η^5 bond in AlCp* is 76.81 kcal/mol, which is almost equal to the M−L BDE in the largest cluster, at 79.72 kcal/mol. Thus, while the M−L bond is slightly weaker in the smaller Al_4 and Al_8 clusters, it has a strength in the largest cluster comparable to that of the monomer. The M−L bond is generally stronger than other aluminum bonding, and it is likely that for all clusters larger than the tetramer the initial unimolecular thermal decomposition step is the removal of AlCp or AlCp* units. Second, functionalizing the Cp ligand reduces the M−L bond strength in comparison to Cp, regardless of cluster size or bond type (η^5 or η^1). The effect is smaller in the half-metallocenes, but in the larger clusters the M−L bonds with Cp* are approximately 33% weaker than those with Cp.

Steric Hindrance. We next briefly consider the steric interactions between the ligand groups in the various clusters. We expect that the ligand bulkiness will play a key role in determining the stability of these compounds against oxidation at atmospheric conditions. It also will have a significant effect on the packing density (and hence the combustion energy density) of these clusters in the solid state, as well as altering the interaction with solvents during crystallization.

To assess the ligand bulkiness and the energy barriers governing steric hindrance between the ligands, we calculate the total energy versus ring slip in the Cp/Cp* clusters. The coordinate for ring slip is taken from ref 19 and is the same as that defined in the previous section. Each slip step corresponds to a 0.5 Å movement of the ligand along the ring slip coordinate, while all other atoms are kept fixed. The 0 Å step begins with the B3LYP optimized geometry, and the energies of subsequent steps result from single-point calculations on the slipped systems. Figure 8 shows energy versus ring slip for the smaller clusters. The methyl groups provide a significant increase in repulsion between adjacent ligands as compared to the nonmethylated Cp. The lone AlCp monomer shows significantly higher energy increases with Cp

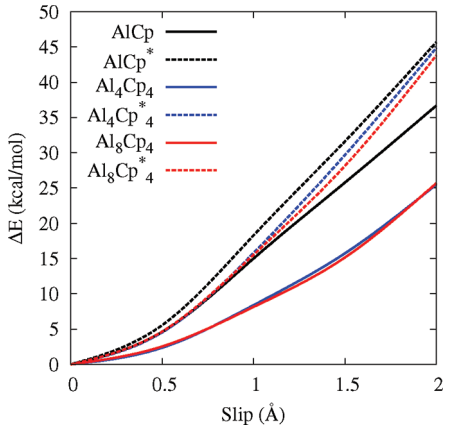

Figure 8. Energy change for smaller clusters as a function of slipping the Cp ligand perpendicular to the Al−η^5 axis.

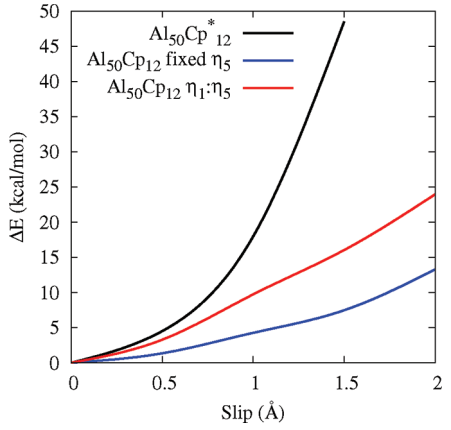

Figure 9. Energy change for ring slippage in the large Al_{50} clusters.

ligand slip as compared to Al_4Cp_4 and Al_8Cp_4 due to a lower M−L bond strength and charge migration to the central Al core in the larger clusters.

The ring slip for the large Al_{50} clusters is shown in Figure 9. For the unmethylated $Al_{50}Cp_{12}$, we consider two structures; first, the cluster in which all ligand groups retain an η^5 bonding as in $Al_{50}Cp^*_{12}$ (denoted as "fixed η_5"), and second, the fully relaxed geometry in which eight of the ligands slip to an η^1 configuration (denoted "η_1/η_5"). The slip values in the latter case are for one of the four ligands remaining in an η^5 bonding. As expected, the large methylated cluster shows significant steric hindrance with slippage, well above that of the unmethylated clusters. Allowing the $Al_{50}Cp_{12}$ ligands to relax into η^1 configurations increases the steric hindrance, suggesting that the mixture of hapticities observed in $Al_{50}Cp_{12}$ may arise largely from ligand steric effects.

The methyl groups in the Cp* ligands add significant steric interaction during ring slippage, but we expect them to generally behave as weakly hindered rotors in the isolated equilibrium cluster configuration. Figure 10 displays the energy barrier required to rotate one methyl group by 60° (half of the symmetry-equivalent rotation of 120°). The points along each curve correspond to B3LYP single-point calculations in which a single methyl group is rotated in 10° steps while all other atoms are again kept fixed. The hindrance is indeed very low; every cluster, regardless of size, has an energy barrier to methyl rotation

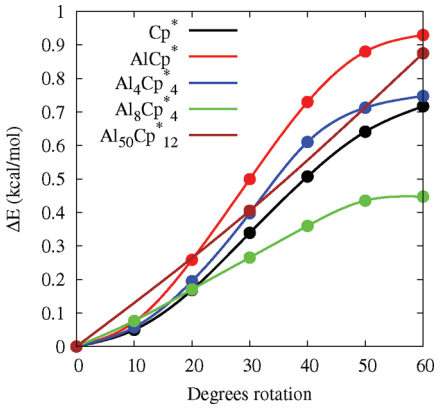

Figure 10. Energy barrier to methyl group rotation on the Cp* ligands of several Al−η^5 clusters.

Table 8. Standard Enthalpies of Formation Calculated Using B3LYP/6-31g(d,p), G2, and B3LYP/6-31g(d,p) at the B3LYP:UFF Geometry

	ΔH_f^0 (kcal/mol)		
cluster	B3LYP	G2	B3LYP:UFF
Al_4 cluster	207.48	178.37	
Cp^-	37.21	34.99	
$[Cp^*]^-$	−5.25		
AlCp[†]	56.94	50.20	
AlCp*	17.51	10.70	16.58
$AlC_5H_4NO_2$	54.84		
$AlC_5Me_4CF_3$	−139.13		
$AlC_5[CF_3]_5$	−739.61		
$AlCp_3$	114.72		
$AlCp_3$*	23.58		
Al_4Cp_4	214.26		
Al_4Cp_4*	61.69		61.68
Al_8Cp_4	341.91		
Al_8Cp_4*	169.62		175.29
$Al_{50}Cp_{12}$	1680		
$Al_{50}Cp_{12}$*			1426

[†] A previous calculated value of 49.4 kcal/mol is given in ref 18.

that is less than 1 kcal/mol. This insensitivity to methyl position justifies our use of the multilayer QM/MM method for geometry optimization which uses UFF for the methyl groups in the largest cluster. Though these groups should properly be treated as free or hindered rotors, their contribution to the partition function of this large cluster is extremely small, and thus, for simplicity, we continue to treat them as vibrations in the thermochemistry calculations discussed below.

Thermodynamics. We next consider the thermochemistry of these compounds, with particular focus on their energy content for propellant and energetic material applications. The standard enthalpies of formation, ΔH_f^0, are shown in Table 8. For smaller clusters G2 calculations were also run to confirm the validity of the B3LYP/6-31G(d,p) basis set in predicting heats of formation. Both the B3LYP and G2 values for AlCp (56.94 and 50.20 kcal/mol, respectively) are close to the previously reported theoretical value of 49.4 kcal/mol.[18] The B3LYP heats of

Table 9. Reactions Involved in the Proposed Stabilization Mechanism in Ref 21

reaction	ΔH^0_{rxn} (kcal/mol)	ref 21 (kcal/mol)
$Al_{50}Cp_{12}^*(g) + 19AlCp_3^*(g) \rightarrow 46Al(s) + 23AlCp_3^*(g)$	−932.3	−473.9
$17.25Al_4Cp_4^*(g) \rightarrow Al_{50}Cp_{12}^*(g) + 19AlCp_3^*(g)$	+809.6	+418.3
$17.25Al_4Cp_4^*(g) \rightarrow 46Al(s) + 23AlCp_3^*(g)$	−122.7	−55.69
$17.25Al_4Cp_4^*(g) \rightleftharpoons 69AlCp^*(g)$	±144.0	±479.0
$Al_4Cp_4^*(g) + 6AlCp^*(g) \rightarrow Al_8Cp_4^*(g) + 2AlCp_3^*(g)$	+50.03	
$Al_{50}Cp_{12}(g) + 19AlCp_3(g) \rightarrow 46Al(s) + 23AlCp_3(g)$	−822.0	−582.2
$17.25Al_4Cp_4(g) \rightarrow Al_{50}Cp_{12}(g) + 19AlCp_3(g)$	+163.7	−1.195
$17.25Al_4Cp_4(g) \rightarrow 46Al(s) + 23AlCp_3(g)$	−658.3	−583.4
$17.25Al_4Cp_4(g) \rightleftharpoons 69AlCp(g)$	±232.9	±638.6
$Al_4Cp_4(g) + 6AlCp(g) \rightarrow Al_8Cp_4(g) + 2AlCp_3(g)$	+15.45	

formation generally tend to uniformly be slightly larger than the G2 value, as do the B3LYP calculations taken at the B3LYP:UFF geometry.

For the largest cluster, $Al_{50}Cp_{12}^*$, we calculated the geometry of the structure by performing a QM/MM calculation using a multilayer ONIOM method as discussed above. The lower ONIOM layer contains the methyl groups treated with UFF, while the Al core and Al−η^5 bonded atoms are treated with B3LYP/6-31G(d,p). Energy differences for the atomization reactions are derived from a full DFT calculation; only the initial geometries are taken from the more computationally efficient QM/MM approach. As discussed above, the overall partition functions are not sensitive to the details of the bulky methyl groups, and separating the system results significantly improved computational times. Similar calculations for $AlCp^*$, $Al_4Cp_4^*$, and $Al_8Cp_4^*$ in Table 8 yield results very close to full DFT and G2 calculations.

We next consider a reaction scheme proposed by Schnöckel and co-workers as an explanation for why $Al_4Cp_4^*$ is sufficiently stable to persist in solution and solid state form, but Al_4Cp_4 is not. They hypothesize that the large Al_{50} clusters serve as a barrier state that the tetramers must pass through before decomposition into a pure metallic phase. The presence of this barrier is suggested to "trap" the tetramer complexes on their way to metallization. In ref 21, these authors present an energy level diagram in which the energy change for an idealized reaction taking Al_4Cp_4 to $Al_{50}Cp_{12}$ and $AlCp_3$ is slightly negative, whereas the analogous reaction in the methylated system is strongly positive. There is not sufficient information to reproduce the energy calculations given in ref 21, as no details are given on the calculated structures, enthalpies of formation, or if the energies are corrected from the bare DFT SCF energy to account for thermal effects. In Table 9, we present our values for the reaction enthalpies in the proposed mechanism, along with the previous values from ref 21. ΔH^0_{rxn} is defined as

$$\Delta H^0_{rxn} = \Delta H^0_f(\text{products}) - \Delta H^0_f(\text{reactants}) \quad (1)$$

All values of ΔH^0_f for the gaseous components (denoted as (g)) are taken from Table 8, and equations involving solid aluminum (denoted Al(s)) are adjusted by an amount equal to the standard enthalpy of vaporization of Al.

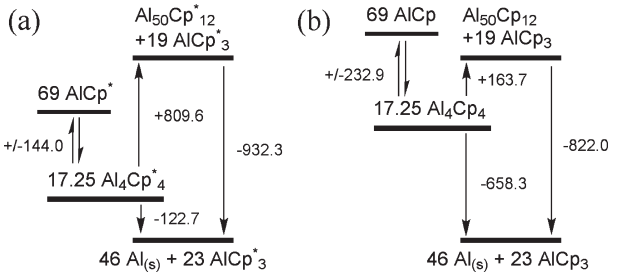

Figure 11. Enthalpies of reaction in kcal/mol for the proposed[21] barrier mechanism with (a) Cp* and (b) Cp ligands.

A visual diagram of our calculated enthalpies of reaction is given in Figure 11. The structure of our energy diagram is mirrored after that proposed by Huber et al. in ref 21, but we find a different trend for the $Al_{50}Cp_{12}$ cluster. Our calculations give a positive ΔH^0_{rxn} of 163.7 kcal/mol for the disproportionation reaction $Al_4Cp_4(g) \rightarrow Al_{50}Cp_{12}(g) + AlCp_3(g)$. In contrast with previous work, the Al_{50} structures are "barrier" states in both the methylated and unmethylated systems, though we do find that this barrier is lower for the Cp clusters than in the Cp*. Additionally, reactions that take the tetramers to the corresponding Al_8 and $AlCp_3$ compounds are positive for both Cp and Cp* ligands. These reactions are not shown in Figure 11 or discussed in ref 21, but they provide further evidence that if one considers the larger clusters to be barrier states to metallization, then they provide a positive energy barrier for both Cp and Cp* based compounds.

In our work we observe significant relaxation of the ligands in the $Al_{50}Cp_{12}$ complex, and it is possible that this is the origin of our disagreement with the previous report, which gives no information on the calculated structure or thermodynamics of $Al_{50}Cp_{12}$. As a check, we have also calculated enthalpies of formation using BP86 with an SVP basis set, similar to the methodology used in previous work.[21] The calculated enthalpies of formation for AlCp and AlCp* with this method are 2.63 and −79.6 kcal/mol, respectively; these differ significantly from G2 and literature values as well as our method, and this may also account for disagreement with previous calculations. The computational scheme used here shows good agreement with G2 results for smaller clusters, and we expect that the heats of

Table 10. Heat of Combustion, Both by Volume and by Mass, For Two Aluminum Organometallic Clusters Compared with Solid Al and Two Standard Energetic Materials

component	ΔH_c (kcal/cm^3)	ΔH_c (kcal/g)	ρ (g/cm^3)
Al	19.99	7.40	2.701
PBX[a]	7.07	4.25	1.664
RDX	3.82	2.11	1.810
$Al_4Cp_4^*$	10.51	9.80	1.072
$Al_{50}Cp_{12}^*$	11.48	9.05	1.269

[a] The PBX compound here represents a simplified aluminized explosive mix of 64% RDX, 20% Al, and the remainder a combination of binder and plasticizer, by weight.

formation will generally be accurate if the cluster geometry is correct. The large idealized reactions in this diagram certainly amplify small changes in the calculated enthalpies of formation of the materials, but overall, the results calculated with our computational methodology do not support the hypothesis of the Al_{50} compound serving as a barrier to immediate metallization of the tetramer. The differences between the Cp and Cp* complexes may instead simply arise from the stabilizing effect of the Cp* methyl groups, which provide a significantly larger steric hindrance in condensed phase environments. We note that in many cases (see Table 7), the Cp variations of a given structure have larger intrinsic bond strengths than those with Cp*. The free energy barriers to decomposition of the Al_4Cp_4 and $Al_4Cp_4^*$ tetramers into monomeric units are both calculated to be negative at ambient conditions, but experimentally the former (unmethylated) decomposes spontaneously and the latter (methylated) is observed up to temperatures beyond 100 °C. This suggests that the steric effects, rather than the innate binding energy of the cluster, are playing a key role in the decomposition. This is consistent with the idea that AlCp or AlCp* removal is the initial decomposition step and that steric hindrance from the ligand is an important limiting mechanism for monomer detachment. We also note that the tetramer $Al_4(C_5Me_4H)_4$, in which each Cp ligand has four methyl groups instead of five as in Cp*, has also been experimentally observed in solid state form, further suggesting the necessity of strong steric hindrance for cluster stability.[14]

Combustion Properties. To evaluate the potential for using these clusters as novel fuel additives or energetic materials, we use the above thermodynamic data to estimate some typical energetic properties. In this section, we focus on two of the clusters in our study that have been successfully synthesized experimentally in small quantities, $Al_4Cp_4^*$ and $Al_{50}Cp_{12}^*$. The heat of combustion, ΔH_c (in kcal/g) for each cluster is calculated using Cheetah 5.0,[36] with the B3LYP heat of formation from Table 8 supplied as input. Cheetah is a chemical equilibrium code that assumes complete chemical reaction of all aluminum clusters in air.[36] This value is then converted to a volumetric heat of combustion using the experimental density of the molecular crystal.[8,9]

Volumetric heats of combustions for each cluster are shown in Table 10, along with values for metallic Al and two explosives, RDX and a representative aluminized explosive formulation denoted PBX. The latter is a mix of 64% RDX, 20% Al, and the remainder a combination of polymeric binder and plasticizers. Despite low densities, the volumetric heats of combustion of the organometallic materials are high, approaching 60% that of pure aluminum due to their high enthalpies of formation, strained aluminum cores, and surrounding hydrogen-rich ligands. This suggests that these materials are very promising as novel fuels or propellants in terms of their raw energy density, if they can be made sufficiently air and temperature stable. We note that a simple analysis of the heat of combustion ignores the differences in the decomposition kinetics of the organometallic aluminum complexes versus standard aluminum powders, which naturally will be very significant. If decomposition proceeds readily through the loss of surface AlCp* layers as discussed above, we expect that the exposed interior core would react on time scales far shorter than the diffusion-limited combustion of large aluminum particles.

Table 11. Specific Impulse of Several Idealized Fuel/Oxidizer Mixtures[a]

mix ratio (%vol)	I_{sp} (sec)
20 Al/80 AP	246
20 $Al_4Cp_4^*$/80 AP	252
40 $Al_{50}Cp_{12}^*$/60 AP	266
20 Al/70 AP/10 HTPB	258
20 $Al_{50}Cp_{12}^*$/70 AP/10 HTPB	260

[a] Each formulation contains a solid fuel (either metallic Al or an Al-based cluster) and is approximately oxygen balanced using AP as an oxidizer.

We next consider the specific impulse I_{sp} of idealized formulations of oxidizers with aluminum−cylcopentadienyl compounds to evaluate their potential use in solid rocket motors. The I_{sp} values given here represent the change in impulse per propellant mass, normalized with the gravitational constant so that the final units are in seconds. The materials are assumed to initially burn in a combustion chamber at a pressure of 1000 psi before expanding isentropically through an ideal rocket nozzle and into an ambient pressure environment. Chemical equilibrium is assumed to hold at every point during the expansion process and the products are allowed to evolve as they expand. The BKWS equation of state[37] is used to calculate chemical equilibrium. In all cases, the oxidizer/organometallic mixture was optimized until the mixture was approximately oxygen balanced; the final compositions are shown in Table 11. The value for a traditional ammonium perchlorate (AP)/aluminum mixture is 246 s, and the organometallic/AP mixtures fall slightly higher than this. A similar trend is observed in a formulation with the common hydroxyl-terminated polybutadiene (HTPB) polymeric binder, where the organometallic provides a comparable I_{sp} to an AP/Al mixture in this simple approximation. Thus, in terms of raw energy content, the organometallic/oxidizer formulations are calculated to provide similar or perhaps slightly superior I_{sp} values in solid rocket motors as compared to high-performance AP/Al mixtures. The significant expected differences in the decomposition kinetics and aluminum oxidation between the organometallics and bulk aluminum are ignored in this analysis; based on the cluster binding energies discussed above, these materials may decompose rapidly enough that the propellant surface area in the motor could be reduced. This might allow, for example, compact end-burner geometries with no central core through the propellant grain.

CONCLUSIONS

We have studied a range of aluminum−cyclopentadienyl cluster compounds using density functional theory to determine their

suitability for use as novel fuels or propellants. The structure and bonding of these clusters was studied in detail, and the organometallic Al−ligand bonds are generally 55−85 kcal/mol and are much stronger than Al−Al interactions. This suggests that thermal decomposition in these clusters will proceed via the loss of surface metal−ligand units, exposing the interior aluminum core. Free energy barriers for removal of these AlCp or AlCp* units are quite low for some of the experimentally observed clusters, indicating that steric effects from the ligand are playing a dominant role in the cluster stability. The energy density of the large clusters, as gauged by their volumetric heat of combustion, is calculated to be nearly 60% that of pure aluminum. These organometallic cluster systems may provide a route to extremely rapid aluminum combustion for use in new fuels and solid rocket propellants.

AUTHOR INFORMATION

Corresponding Author
*E-mail: jphooper@nps.edu.

ACKNOWLEDGMENT

The authors would like to acknowledge Jim Lightstone, Chad Stoltz, Becca Wilson, and Patrick Holvey for valuable discussions. This work was supported by the Defense Threat Reduction Agency (DTRA) Grant 11-2818M. K.S.W. acknowledges support provided by the Office of Naval Research through its Naval Research Enterprise Intern Program.

REFERENCES

(1) Armstrong, R. W.; Baschung, B.; Booth, D. W.; Samirant, M. *Nano Lett.* **2003**, *3*, 253–255.
(2) Trunov, M. A.; Umbrajkar, S. W.; Schoenitz, M.; Mang, J. T.; Driezen, E. L. *J. Phys. Chem. B* **2006**, *110*, 13094–13099.
(3) Jouet, R. J.; Warren, A. D.; Rosenberg, D. M.; Bellitto, V. J.; Park, K.; Zachariah, M. R. *Chem. Mater.* **2005**, *17*, 2987–2996.
(4) Chung, S. W.; Guliants, E.; Bunker, C.; Hammerstroem, D.; Deng, Y.; Burgers, M.; Jelliss, P.; Buckner, S. *Langmuir* **2009**, *25*, 8883–8887.
(5) Meziani, M. J.; Bunker, C.; Lu, F.; Li, H.; Wang, W.; Guliants, E.; Quinn, R.; Sun, Y. *ACS Appl. Mater. Interfaces* **2009**, *1*, 703–709.
(6) Lewis, W. K.; Rosenberger, A.; Gord, J.; Crouse, C.; Harruff, B.; Fernando, K.; Smith, M.; Phelps, D.; Spowart, J.; Guliants, E.; Bunker, C. *J. Phys. Chem. C* **2010**, *114*, 6377–6380.
(7) Beckstead, M. W.; Newbold, B. R.; Waroquet, C. Proceedings of the 37th JANNAF Combustion Meeting, Monterey, CA, 2000; Chemical Propulsion Information Analysis Center: Columbia, Maryland, Vol *1*, p 492.
(8) Vollet, J.; Hartig, J. R.; Schnöckel, H. *Angew. Chem., Int. Ed.* **2004**, *43*, 3186–3189.
(9) Dohmeier, C.; Robl, C.; Tacke, M.; Schnöckel, H. *Angew. Chem., Int. Ed.* **1991**, *30*, 564–565.
(10) Schnöckel, H.; Köhnlein, H. *Polyhedron* **2002**, *21*, 489–501.
(11) Dohmeier, C.; Loos, D.; Schnöckel, H. *Angew. Chem., Int. Ed.* **1996**, *35*, 129–149.
(12) Schnepf, A.; Schnöckel, H. *Angew. Chem., Int. Ed.* **2002**, *41*, 3532–3554.
(13) Schnöckel, H. *Chem. Rev.* **2010**, *110*, 4125–4163.
(14) Huber, M.; Schnöckel, H. *Inorg. Chim. Acta* **2008**, *361*, 457–461.
(15) Bono, D.; Hartig, J.; Huber, M.; Schnöckel, H.; Jongh, L. *J. Cluster Sci.* **2007**, *18*, 319–331.
(16) Ahlrichs, R.; Ehrig, M.; Horn, H. *Chem. Phys. Lett.* **1991**, *183*, 227–233.
(17) Gauss, J.; Schneider, U.; Ahlrichs, R.; Dohmeier, C.; Schnöckel, H. *J. Am. Chem. Soc.* **1993**, *115*, 2402–2408.
(18) Rayón, V. M.; Frenking, G. *Chem.—Eur. J.* **2002**, *8*, 4693–4707.
(19) Budzelaar, P. H. M.; Engelberts, J. J.; van Lenthe, J. H. *Organometallics* **2003**, *22*, 1562–1576.
(20) Alary, F.; Heully, J.-L.; Poteau, R.; Maron, L.; Trinquier, G.; Daudey, J.-P. *J. Am. Chem. Soc.* **2003**, *125*, 11051–11061.
(21) Huber, M.; Henke, P.; Schnöckel, H. *Chem.—Eur. J.* **2009**, *15*, 12180–12183.
(22) Becke, A. D. *J. Chem. Phys.* **1993**, *98*, 5648–5652.
(23) Curtiss, L. A.; Raghavachari, K.; Trucks, G. W.; Pople, J. A. *J. Chem. Phys.* **1991**, *94*, 7221–7230.
(24) Frisch, M. J. et al. *Gaussian 09*, Revision A.1; Gaussian Inc.: Wallingford, CT, 2009.
(25) Dapprich, S.; KomĞromi, I.; Byun, K. S.; Morokuma, K.; Frisch, M. J. *J. Mol. Struct.: THEOCHEM* **1999**, 1–21.
(26) Rappe, A. K.; Casewit, C. J.; Colwell, K. S.; Ill, W. A. G.; Skiff, W. M. *J. Am. Chem. Soc.* **1992**, 10024–10035.
(27) Haaland, A.; Martinsen, K.-G.; Shlykov, S. A.; Volden, H. V.; Dohmeier, C.; Schnöckel, H. *Organometallics* **1995**, *14*, 3116–3119.
(28) K., K.; Burgert, R.; Stösser, G.; Schnöckel, H. *Eur. J. Mass Spectrom.* **2005**, *11*, 469–474.
(29) Rao, B. K.; Jena, P. *J. Chem. Phys.* **1999**, *111*, 1890–1904.
(30) Schnöckel, H.; Schnepf, A.; Whetten, R. L.; Schenk, C.; Henke, P. *Z. Anorg. Allg. Chem.* **2011**, *637*, 15.
(31) Beswick, M. A.; Palmer, J. S.; Wright, D. S. *Chem. Soc. Rev.* **1998**, *27*, 225–232.
(32) Dapprich, S.; Frenking, G. *J. Phys. Chem.* **1995**, *99*, 9352–9362.
(33) Frenking, G.; Wichmann, K.; Frohlich, N.; Loschen, C.; Lein, M.; Frunzke, J.; Rayon, V. M. *Coord. Chem. Rev.* **2003**, *238−239*, 55–82.
(34) Lopez-Acevedo, O.; Clayborne, P. A.; Hakkinen, H. *Phys. Rev. B* **2011**, *84*, 035434.
(35) Clayborne, P.; Lopez-Acevedo, O.; Whetten, R. L.; Grönbeck, H.; Häkkinen, H. *J. Chem. Phys.* **2011**, *135*, 094701.
(36) Bastea, S.; Fried, L.; Glaesemann, K.; Howard, W. M.; Souers, P. C.; Vitello, P. A. *Cheetah 5 User's Manual*; Lawrence Livermore National Laboratory: Livermore, CA, 2007.
(37) Mader, C. *Detonation Properties of Condensed Explosives Computed Using the Becker-Kistiakowsky-Wilson Equation of State*; Los Alamos National Laboratory: Los Alamos, NM, 1963; LA-2900.